RSC Advances

ROYAL SOCIETY OF CHEMISTRY

www.rsc.org/advances

MOLECULAR PHOTO-THERMAL OPTICAL COHERENCE PHASE MICROSCOPY USING GOLD NANORODS

Jing-Hong Pai[1,2], Tianqing Liu[2], Hung-Yao Hsu[1], A. Bruce Wedding[1], Benjamin Thierry[2,*], Pierre Bagnaninchi[3,*]

[1] School of Engineering, University of South Australia, Mawson Lakes, SA 5095, Australia

[2] Ian Wark Research Institute, University of South Australia, Mawson Lakes, SA 5095, Australia

[3] MRC Centre for Regenerative Medicine, University of Edinburgh, EH16 4UU, United Kingdom

*Corresponding author:

Email Benjamin.thierry@unisa.edu.au

Email Pierre.bagnaninchi@ed.ac.uk

Abstract

Optical coherence tomography (OCT) is a non-invasive interferometry imaging technique with micrometre scale resolution at millimetre scale penetration depths in highly scattering tissues. This study describes a new evolution of OCT, termed molecular optical coherence phase microscopy (molecular OCPM), which is capable of imaging expression of molecular markers at the cellular level using gold nanorods as photothermal imaging agents. Gold nanorods were selected as the imaging agents due to their excellent photothermal energy conversion efficiency and tuneable plasmon bands. The gold nanorods were surface functionalized to achieve efficient and specific targeting of the tyrosine kinase human epidermal growth factor receptor HER2 molecular markers used as a model tumor biomarker. Phase modulation retrieval was used to generate photothermal maps which were overlayed to intensity images. Phase modulation within the filter corresponding to the laser excitation modulation frequency was clearly observed for cells targeted with the molecular photothermal imaging agents. These results confirm the ability of photothermal optical coherence phase microscope to image accurately at the cellular level gold nanorods molecularly targeted to a biomarker expressed on cancer cell membranes, paving the way for its application to novel bioimaging procedures.

Introduction

Optical coherence tomography (OCT) is a label-free and non-invasive interferometry imaging modality[1,2] that bridges the gap between microscopy and ultrasound achieving micrometre scale resolution at millimetre scale penetration depths in highly scattering tissues. OCT maps in-depth the difference in optical scattering, and thus relies on endogenous microstructural contrast to image the material under investigation. Both the amplitude and the phase of the interferometric signal can be retrieved with an acquisition speed allowing video-rate imaging. OCT is suitable for *ex vivo* and *in vivo* imaging through intravital imaging windows or endoscopes.[3] It has been established as a clinical standard in ophthalmology[4], and adopted for clinical applications in cardiology[5] and gastroenterology. The growing potential of optical coherence tomography in preclinical cancer imaging has been recently evidenced with exciting opportunities in the monitoring of cancer treatments.[6]

Generally OCT sacrifices lateral resolution to achieve deep imaging in tissues, however axial and lateral cellular resolution can be achieved by combining microscopy objectives and the optical coherence tomography principle.[7-9] In addition, an interferometer in a common-path configuration can be implemented to perform quantitative phase-contrast imaging with unmatched sensitivity that enables single-cell mapping and the detection of nanometer-level fluctuations.[10,11] We recently demonstrated that this modality, common-path optical coherence phase microscopy (OCPM), was able to record phase fluctuations associated with the motility of viable cells in two dimensions (2D) and 3D.[12-14]

Although the label-free nature of OCT has been one of the main driving forces for its widespread adoption in biomedical sciences, the inability to use molecular probes to label cells and molecules has become a limitation towards the application of OCT in clinical investigation. The recent demonstration of the possibility to use plasmonic nanoparticles as photothermal probes for OCT [15-20] , as well as organic polymer nanoparticles [21,22], represents

a paradigm shift in the field, paving the way to molecular optical imaging in deep tissues. OCT contrast provides tissue imaging at millimetre depth whilst plasmonic nanoparticles functionalized with biological ligands have the potential to enable localization of molecular markers of interest *in vitro* and *in vivo.* At wavelengths specific to the absorption band of the nanoparticles, energy is absorbed due to plasmonic confinement and released in the form of heat, generating a signal measurable by OCT as a localized change in optical properties.[23] The photothermal effect associated with plasmonic nanoparticles has already been successfully used to develop contrast agents for photoacoustic imaging.[24-26]

Despite its promise, photothermal bioimaging is still in its infancy; the development of efficient molecularly targeted photothermal imaging agents combined with the establishment of robust imaging protocols is required for this novel technology to be adapted by biologists. To this end, we demonstrate the possibility to use photothermal OCPM for taking the images of gold nanorods target to proto-oncogene tyrosine kinase human epidermal growth factor receptor HER2 associated with aggressive breast cancer. The demonstration of the feasibility to image, at a cellular resolution, specific biomarkers expressed in biological tissues using OCPM is a step towards the implementation of this promising technology in biomedical imaging.

Materials and Methods

Photothermal Optical Coherence Phase Microscopy System

The system used in this study was described in detail previously[12]. The system is built around a commercial OCT spectrometer (Callisto, Thorlabs) equipped with a superluminescent laser diode (SLD) light source centred at λ_o= 930 nm with a FWHM bandwidth of 90 nm, providing a resolution of 5 μm in tissue. The outgoing laser beam is collimated then incident onto a pair of galvanometers forming, together with a scan lens, a custom laser scanning head (LSH) that raster the beam to the lens tube of an inverted microscope (SPi95, Brunel). In this study a 10x objective (NA=0.17) with in a 1.5 micrometre lateral resolution was used. The system was in a common path configuration where the first reflection from the sample was used as a reference, in this case the bottom of the glass slide where cells where were cultured. The common path configuration resulted in increased phase stability rejecting common noise more efficiently.

At each x,y point of the sample a spectrum was collected at a rate of 1200 spectra per second. Intensity and phase information along the depth axis, Z, were retrieved by fast Fourier transform of the spectra but only the signal corresponding to the glass slide was represented to provide an en-face image of the sample. In addition, we recorded successive B scans at the same location with an acquisition frequency of 3 Hz to measure phase modulation resulting from the photothermal effect. En face imaging of 2D cell culture was performed by collecting 200 scans in both the X and Y directions and by repeating the B scan collection at the Y position 50 times.

In the inverted microscope configuration we made use of the illumination path to insert an 808nm laser diode as the excitation laser. The laser was coupled in and out of the optical axis at low frequency with a galvanometer mirror to allow B scan photothermal mode. The laser

diode was coupled in and out of the optical axis every 4 seconds, resulting in a modulation frequency of 0.125 Hz.

Synthesis and Biofunctionalization of the Gold Nanorods

Gold nanorods were prepared using the standard seed-mediated method in the presence of the cationic surfactant cetyltrimethylammonium bromide (CTAB). Gold seeds were prepared by mixing an aqueous CTAB solution (0.2 M, 5.0 mL) with 0.5 mM $HAuCl_4$ (5.0 mL) prior to the addition of ice-cold 0.01 M $NaBH_4$ (0.6 mL). A growth solution was prepared by mixing CTAB (0.2 M, 10.0 mL) with 1.0 mM $HAuCl_4$ (10.0 mL) and various amounts of $AgNO_3$ (0.1 M). Ascorbic acid (78.8 mM, 1.4 mL) was then added as a mild reducing agent, which resulted in the disappearance of the colour of the growth solution. The brownish-yellow seed solution was added under strong agitation to the growth solution. The reaction was left to proceed for 24 hours at 28ºC and the rod solutions were purified by centrifugation at 7500 rpm for 10 minutes and resuspended in MilliQ water. Extinction coefficients determined experimentally by Orendorff *et al.* [27] were used to calculate the concentration of gold nanorods.

To functionalize the gold nanorods with herceptin while preserving the colloidal stability of the nanoparticles, a thiolated polyethyleneglycol adlayer was used based on our previous studies.[28,29] Mixed thiolated PEG molecules comprising carboxylic functionalized short chain length PEG molecules (Fw 458.6) and PEG with longer chain length (Fw 5000) were prepared at a concentration of 1 mg/mL and a molar ratio of 1:2 (Fw 5000: Fw 458.6). 400 µL of the mixed PEG solution was added to the same volume of 1 nM gold nanorod solution under vortex and left to react for at least 6 hours at 4°C. The terminal carboxyl groups on the PEG molecules were activated using 150 µL mixture solution of NHS (20 mg/mL) and EDC (15 mg/mL) for 5 minutes. The nanoparticle suspension was then quickly centrifuged at 8500

rpm and resuspended into PBS. Herceptin antibody or nonspecific IgG1 isotype control antibody (0.5 mg/mL, 0.1 mL) was added rapidly to the activated gold nanorods and left to react at room temperature for 1 hour then washed with PBS twice and stored at 4^{o}C prior to use. Gold nanorods were characterized using UV-Vis spectroscopy (Thermo Scientific Evolution 201 UV/Vis).

Cell Culture and Immune-targeting

The Human breast cancer cell line MCF-7 was obtained from American Type Culture Collection (ATCC, USA). The cells were cultured in complete media, Dulbecco's modified eagle medium (DMEM), supplemented with glutamine and 10% (v/v) fetal bovine serum (FBS; 10082) at 37°C in a 100% humidified incubator with 5% CO_2. Cells were plated in custom-made silicone wells made using polydimethylsiloxane (Sylgard 184 silicone elastomer kit) mounted on glass coverslips treated with poly-D-lysine at densities of 5,000-cells per well (60% confluence). After 24 hours incubation, the cells were incubated for 1 hour at 37°C with 20 µL of the gold nanorods conjugated with either Herceptin or the nonspecific IgG1 isotype control antibody. Cells were then extensively washed in PBS and fixed with cold methanol prior to being mounted for dark-field microscopy and OCPM measurements. The binding of the herceptin targeted gold nanorods to the MCF-7 cells was confirmed using a Nikon TE inverted light microscope operating in bright field and dark-field modes.

Results and Discussion

Molecular Targeting of Gold Nanorods with LSPR Tuned at ~808 nm to Breast Cancer Cells

In this work, functionalized gold nanorods with a longitudinal localised surface plasmon resonance (LSPR) close to 808 nm were used as molecular photothermal agents. The gold nanorods LSPR was selected so that the external laser used to excite the nanorods was compatible with the wavelength of the laser diode used in the OCPM set up. Plasmonic confinement in gold nanorods results in strong light scattering and nonradiative absorption, which can be efficiently converted into heat. This photothermal effect has been widely investigated towards the design of novel imaging and therapeutic approaches[30-32]. In the application of molecular photothermal OCPM for detecting targeted gold nanorods, the plasmonic gold nanorods were conjugated with the monoclonal antibody Herceptin. Gene amplification of the HER2 gene in breast cancer and resulting over-expression of the proto-oncogene tyrosine kinase human epidermal growth factor receptor HER2 occurs in 20% to 30% of patients and is typically associated with an aggressive disease course and poor prognosis.[33,34] Many HER2 targeted nanoparticle based diagnostic molecular strategies are therefore under development.[35] For instance, HER2 targeted gold nanoparticles could enhance the visibility of tumour peripheries and enable detection of millimetre-sized tumours in an animal model using microCT.[36] Molecular photoacoustic imaging was also successfully achieved using HER2 targeted gold nanorods.[37]

Gold nanoparticles are prone to aggregation in biological milieu as well as during bioconjugation with biological ligands. In addition, non-specific binding to cells leads to increase signal-to-noise and in turn decreased sensitivity in molecular imaging.[38] Efficient biointerfaces are therefore required to reach the full potential of nanoscale molecular imaging agents. Building on our previous studies[28], a mixed PEG adlayer designed to maximize the colloidal stability and bioconjugation was introduced on the gold nanoparticles, displacing

the native CTAB layer.[28,39] After carbodiimide activation of free terminal carboxyl groups on the PEG adlayer, the nanorods were reacted with the monoclonal antibodies and purified. No discoloration of the nanorods solutions was observed during the bioconjugation steps, suggesting that the nanoparticles were aggregation-free. This was confirmed using UV-Vis spectroscopy, where no significant broadening of the longitudinal plasmon band could be observed for the gold nanorods (Figure 1.a). In addition, a red-shift of the longitudinal plasmon band was observed after conjugation with herceptin to the PEG adlayer, suggesting the efficient conjugation of the proteins.

The human breast adenocarcinoma cancer cells MCF-7, which over-express the HER2 receptor, were used as a model for herceptin expressing cancerous tissues. Cells plated in custom made silicon chambers mounted onto coverslips were incubated for 60 minutes at room temperature with either the herceptin-conjugated nanorods or nanorods conjugated with a nonspecific IgG1 isotype antibody used as control. Dark-field microscopy was used to demonstrate successful targeting of the breast cancer cells. Strong signals were observed for the cells treated with the herceptin-conjugated gold nanorods as shown in Figure 1.b. On the other hand, cells treated with the non-targeted nanorods displayed only background signal, which confirmed the efficiency and specificity of the molecular gold nanorods probes (Figure 1.c).

Optical Phase Coherence Microscopy Imaged Phase Modulations during Photothermal Excitation with a Cellular Resolution.

In photothermal optical phase coherence microscopy, a low coherence laser beam is sent to a beam splitter and scanned in X and Y directions through the optics of an inverted microscope (Figure 2). The first reflection of a cover slip is used as a reference beam insuring high phase stability. The theoretical stability of our system in air is approximately 7×10^{-5} radians. Cells

seeded on a glass coverslip resulted in a high experimental SNR of 60 db and associated phase stability of 0.001 rad as calculated from equation 4 of reference 11. This high phase stability enabled to operate the photothermal OCPM in a B scan repetition mode as opposed to common usage of the photothermal OCT looking at phase modulation along A-scan repetition. As a result we were able to reduce drastically the number of data points, and to directly display the photothermal phase image comprising 200 sets of 50 B scan repetitions of 200 A scan each both in intensity (Figure 3.a) and in phase (Figure 3.b).

Both intensity and phase images clearly showed the MCF-7 cells over the coverslip background, and phase roughness associated with internal cell microstructure was observed. Details of the phase picture (Figure 3.c) revealed blocks of 50 pixels in the y-direction that represents the time varying phase at the (x,y) location along 50 time points with an acquisition frequency of 3 Hz. In some of these block pixels the phase was found cyclically modulated during photothermal imaging of cells targeted with gold nanorods, as demonstrated in the insert of Figure 3.c.

Photothermal Induced Phase Modulation Matched Excitation Laser Modulation

Figure 4 shows typical plots of the time varying phase within block pixels corresponding to an area without cells (Figure 4.a), to an area with cells but no apparent phase fluctuations (Figure 4.b), and to an area with cells and clear phase modulation (Figure 4.c). Phase variations in Figure 4.a and 4.b were found of similar value if not for a slight increase in phase standard deviation in Figure 4.b that can be attributed to a small decrease in the signal to noise ratio compared to the bare coverslip.

The signal displayed in Figure 4.c was modulated with a frequency matching the excitation laser modulation frequency. Therefore the presence of phase modulation in a 50-pixel block could be attributed to the presence of gold nanorods at the corresponding (x,y) location.

Photothermal optical coherence phase microscopy located immunotargeted gold nanorods in cancer cells

Each photothermal image was block processed in the y-direction with a block size corresponding to the number of times a B scan is repeated, and fast Fourier transform was performed and filtered around the frequency resulting from the laser being turned on and off every 4 seconds. After additional threshold in the Fourier space, we generated the photothermal map of the gold nanorod location. In order to map the immunotargeted gold nanorods in cancer cells a RGB picture was generated with the intensity image on the red channel and the photothermal signal on the green channel. Figure 5 presents the different stages of photothermal optical coherence phase microscopy for both cells without nanorods (Figures 5.a-c) and cells with nanorods (Figures 5.e-g).

OCPM was able to image the cells at a cellular resolution in the intensity mode (Figures 5.a and e). For the sake of clarity, locations were chosen where cells were only partially confluent. No major difference in phase or intensity was observed as a result of the presence of the immunotargeted gold nanorods in the cells. Phase modulation retrieval generated the photothermal map (Figures 5.b and f). The control without the presence of gold nanorods did not show any phase modulation around the chosen filter corresponding to the laser excitation modulation frequency. On the contrary, Figure 5.e revealed the presence of phase modulation associated with the presence of nanoparticles in several locations. When overlayed onto the intensity images, these locations corresponded to location within cancer cells, with the exception of some artefacts. An overlay map of cells without gold nanorods is presented, confirming the ability of photothermal optical coherence phase microscopy to image accurately gold nanorods molecularly targeted to a biomarker expressed on cancer cell membranes. The experimental data presented here has been conducted using fixed cells to

facilitate the validation of the methodology. However, the proposed concept of molecular OCPM would be readily applicable to the imaging of live cells and tissues.

Photothermal imaging is a fast emerging technology in the biomedical community. To the best of our knowledge, there is to date only one published study reporting on the combined use of optical coherence microscopy and photothermal probes, with the advantage over laser scanning microscopy to allow imaging in deep tissue. Pache *et al.* [18] reported for the first time the photothermal imaging of non-functionalised 40nm gold nanoparticles at cellular resolution excited at 532nm with optical coherence microscopy. Previous studies also reported on the possibility to image tissues without cellular resolution with optical coherence tomography[15-17,19].

The study reports for the first time the photothermal imaging of molecularly targeted gold nanorods. Importantly, gold nanorods can be excited in the near infrared part of the spectra (808nm in this study) and their absorption peak can be tuned by varying the length to width ratio. As opposed to spherical gold nanoparticles absorbing broadly around 532nm, narrow tunable absorption in the NIR paves the way towards deep tissue imaging and multiplexed photothermal imaging for simultaneous imaging of several biomarkers of interests. Photothermal optical coherence tomography of the passive uptake of gold nanorods in sentinel lymph node has been demonstrated with tissue-scale resolution [16]. Similarly Tucker-Schwartz *et al.* [19] demonstrated photothermal imaging of non-targeted gold nanorods with OCT.

Conclusion

In this study, we demonstrated for the first time the feasibility to image, at a cellular resolution, specific biomarkers expressed in biological tissues using optical coherence phase microscopy and functionalized gold nanorods as molecular photothermal imaging agents. The

proto-oncogene tyrosine kinase human epidermal growth factor receptor HER2 could be imaged specifically using herceptin-conjugated gold nanorods and photothermal optical coherence phase microscopy. An efficient biointerface was first introduced on the gold nanorods based on a PEG adlayer that maximized colloidal stability and bioconjugation, thereby enabling efficient and specific targeting to HER2 overexpressing cells. Gold nanorods were selected as the OCPM molecular agents due to their excellent photothermal energy conversion efficiency. Importantly, the plasmon bands of gold nanorods can be easily tuned by altering their aspect ratios. Very distinct peaks of absorption can therefore be achieved with minimum overlap, paving the way towards multiplexed photothermal imaging. Plasmon bands in the NIR present an additional advantage in regards to *in vivo* applications of OCPM through intravital windows where NIR light can penetrate more deeply into tissues.

Acknowledgements

This work was supported by the NH&MRC project grant 511303. B. Thierry is supported by a NH&MRC CDA. This work was performed in part at the South Australian node of the Australian National Fabrication Facility, a company established under the National Collaborative Research Infrastructure Strategy to provide nano and micro-fabrication facilities for Australia's researchers.

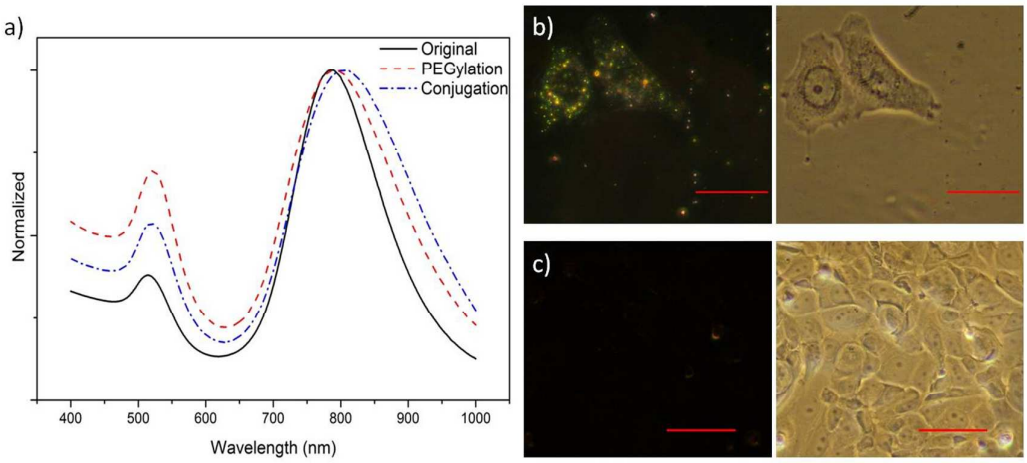

Figure 1. a) UV-visible absorption spectrum of the as-synthesized, PEGylated, and Herceptin-conjugated gold nanorods. Dark field and corresponding bright field microscopy images of MCF-7 cells after incubation with gold nanorods conjugated with **b)** herceptin-conjugated gold nanorods and **c)** a nonspecific IgG1 isotype antibody. Scale bars: 50 µm.

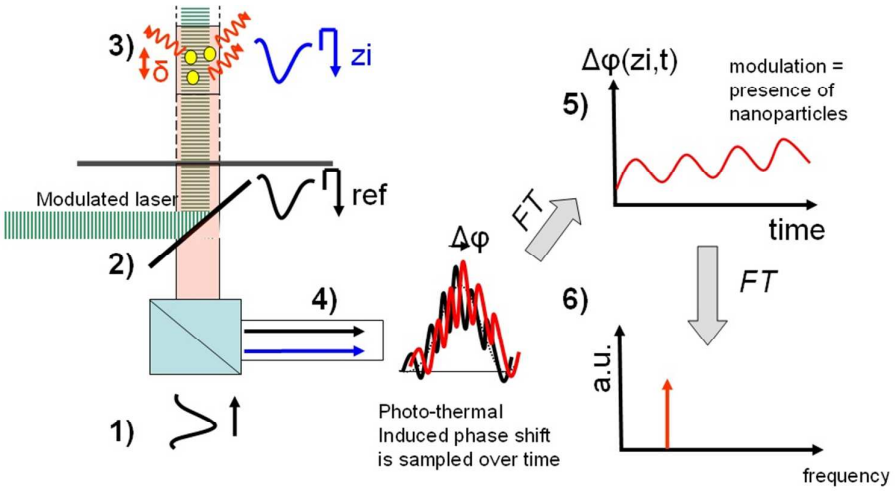

Figure 2. Principle of photothermal optical coherence phase microscopy. **1)** A low coherence laser beam, with a centre wavelength λ_o and a bandwidth $\Delta\lambda$, is sent to a beam splitter and scanned across a sample in X and Y directions. **2)** A dichroic mirror is used to combine the scanning laser with an excitation laser modulated at a frequency. **3)** Nanoparticles absorb and release (heat) energy from the modulated excitation laser. A small periodic change in the optical path is generated when particles are present. **4)** The reference and sample beams recombine in the beam splitter and spectral interferences are recorded. When collected over time, a phase shift related to the change in optical path generated by the photo thermal effect is observed. **5)** When plotted over time the phase associated with a pixel containing nanoparticles is modulated at the excitation laser modulation frequency. **6)** A Fourier transform of the time-varying phase filtered around the excitation frequency determines the presence or not of the particle.

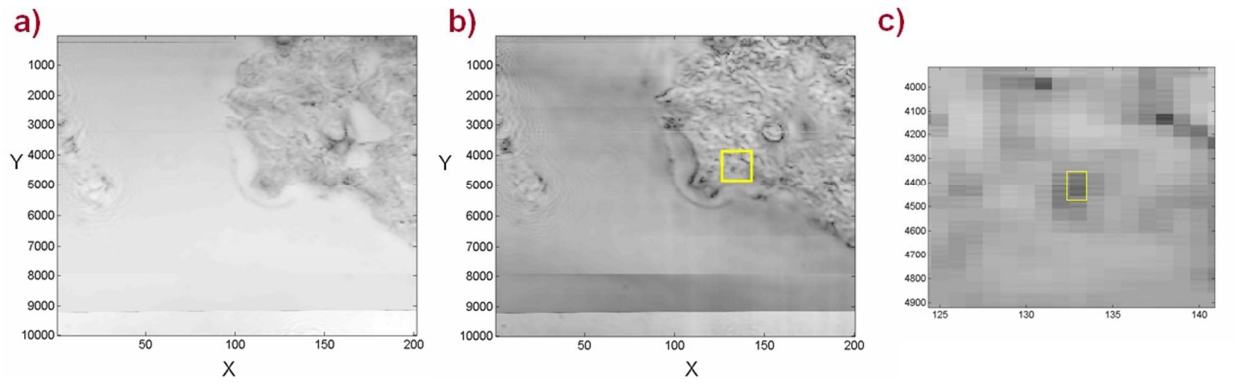

Figure 3. a) Intensity and **b)** phase images generated by the PT-OCT. Images are 10000 x 200 pixels, and equal to 300 µm x 300 µm (1.5 µm separation scan in x,y). The Y direction represents 200 B scans repeated 50 times at the same location to measure time-varying change in phase. **c)** Close up of the marked area in the phase image showing clear signal modulation in some of the 50 pixels blocks.

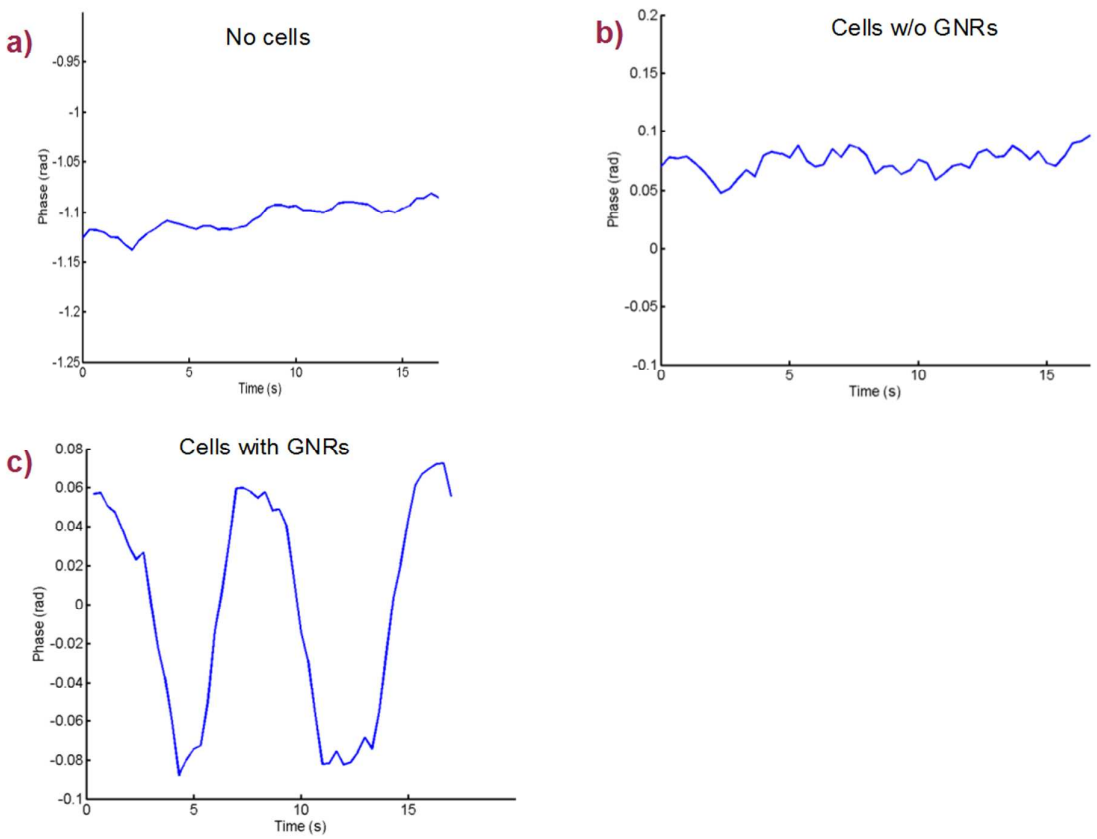

Figure 4. Time varying phase (rad) along 50 B-scans repetitions sampled at 3Hz acquired by the photothermal optical coherence phase microscope for **a)** an area without cells, **b)** an area with cells but no apparent modulation, and **c)** an area with cells and a clear phase modulation matching the excitation laser modulation frequency

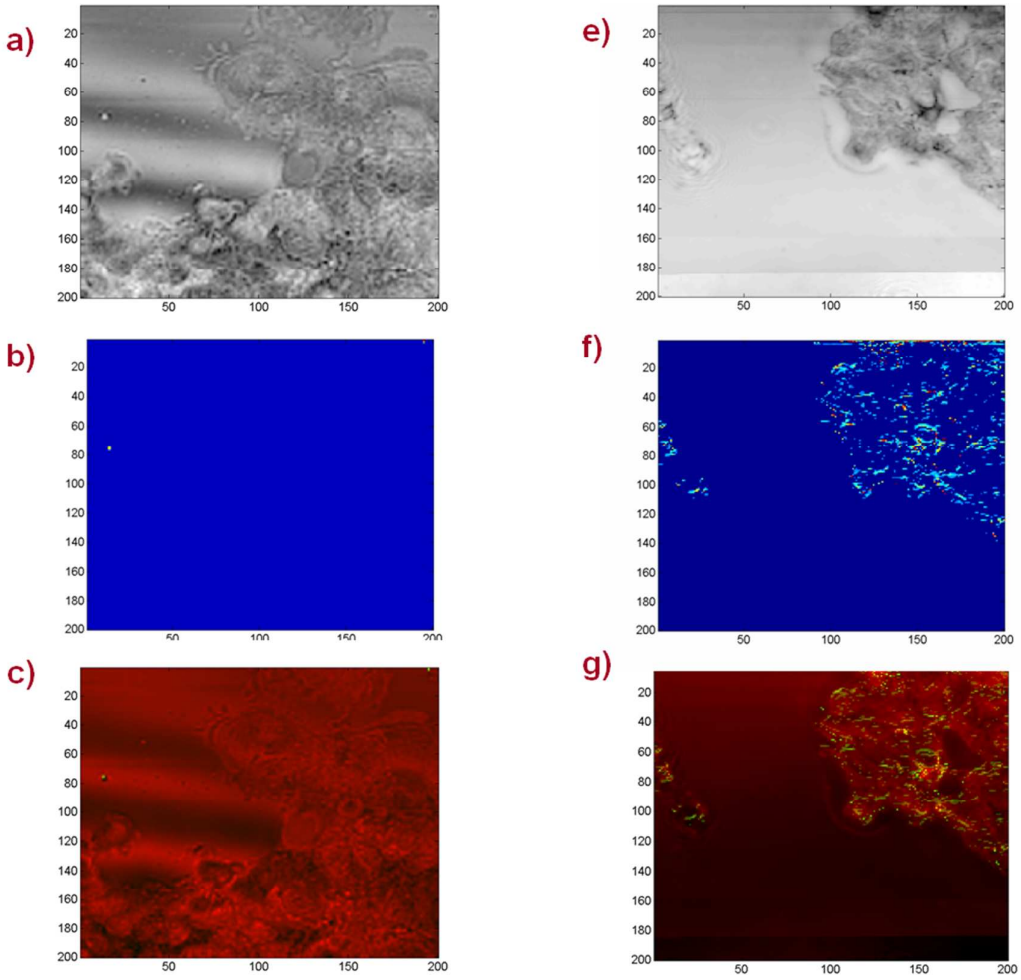

Figure 5. Photothermal optical coherence phase microscopy of immunotargeted gold nanorods. a) - c) Control cells, and e) - g) cells labelled with gold nanorods.

References

(1) Huang, D.; Swanson, E. A.; Lin, C. P.; Schuman, J. S.; Stinson, W. G.; Chang, W.; Hee, M. R.; Flotte, T.; Gregory, K.; Puliafito, C. A. *Science* **1991**, *254*, 1178.

(2) Fujimoto, J. G.; Brezinski, M. E.; Tearney, G. J.; Boppart, S. A.; Bouma, B.; Hee, M. R.; Southern, J. F.; Swanson, E. A. *Nature medicine* **1995**, *1*, 970.

(3) Fujimoto, J. G. *Nat Biotech* **2003**, *21*, 1361.

(4) Drexler, W.; Morgner, U.; Ghanta, R. K.; Kärtner, F. X.; Schuman, J. S.; Fujimoto, J. G. *Nature medicine* **2001**, *7*, 502.

(5) Suter, M. J.; Nadkarni, S. K.; Weisz, G.; Tanaka, A.; Jaffer, F. A.; Bouma, B. E.; Tearney, G. J. *JACC: Cardiovascular Imaging* **2011**, *4*, 1022.

(6) Vakoc, B. J.; Fukumura, D.; Jain, R. K.; Bouma, B. E. *Nature Reviews Cancer* **2012**, *12*, 363.

(7) Aguirre, A.; Hsiung, P.; Ko, T.; Hartl, I.; Fujimoto, J. *Optics Letters* **2003**, *28*, 2064.

(8) Huang, S.-W.; Aguirre, A. D.; Huber, R. A.; Adler, D. C.; Fujimoto, J. G. *Optics Express* **2007**, *15*, 6210.

(9) Lee, H.-C.; Zhou, C.; Cohen, D. W.; Mondelblatt, A. E.; Wang, Y.; Aguirre, A. D.; Shen, D.; Sheikine, Y.; Fujimoto, J. G.; Connolly, J. L. *The Journal of urology* **2012**, *187*, 691.

(10) Choma, M. A.; Ellerbee, A. K.; Yang, C.; Izatt, J. A.; Creazzo, T. L. *Optics Letters* **2005**, *30*, 1162.

(11) Joo, C.; Akkin, T.; Cense, B.; Park, B. H.; de Boer, J. F. *Optics Letters* **2005**, *30*, 2131.

(12) Bagnaninchi, P. O.; Holmes, C.; Drummond, N.; Daoud, J.; Tabrizian, M. *Journal of Biomedical Optics* **2011**, *16*.

(13) Holmes, C.; Tabrizian, M.; Bagnaninchi, P. O. *Journal of Tissue Engineering and Regenerative Medicine* **2013**.

(14) Holmes, C.; Daoud, J.; Bagnaninchi, P. O.; Tabrizian, M. *Advanced healthcare materials* **2013**.

(15) Adler, D. C.; Huang, S.-W.; Huber, R.; Fujimoto, J. G. *Optics Express* **2008**, *16*, 4376.

(16) Jung, Y.; Reif, R.; Zeng, Y.; Wang, R. K. *Nano Letters* **2011**, *11*, 2938.

(17) Skala, M. C.; Crow, M. J.; Wax, A.; Izatt, J. A. *Nano Letters* **2008**, *8*, 3461.

(18) Pache, C.; Bocchio, N. L.; Bouwens, A.; Villiger, M.; Berclaz, C.; Goulley, J.; Gibson, M. I.; Santschi, C.; Lasser, T. *Optics Express* **2012**, *20*, 21385.

(19) Tucker-Schwartz, J.; Meyer, T.; Patil, C.; Duvall, C.; Skala, M. *Biomedical optics express* **2012**, *3*, 2881.

(20) Kim, C. S.; Wilder-Smith, P.; Chen, Z.; Kwon, Y. J.; Ahn, Y.-C.; Liaw, L.-H. L. *BIOMEDO* **2009**, *14*, 034008.

(21) Kasaragod, D.; Au, K. M.; Lu, Z.; Childs, D.; Armes, S. P.; Matcher, S. J. 2013; Vol. 8596, p 85960R.

(22) Au, K. M.; Lu, Z.; Matcher, S. J.; Armes, S. P. *Adv. Mater.* **2011**, *23*, 5792.

(23) Boyer, D.; Tamarat, P.; Maali, A.; Lounis, B.; Orrit, M. *Science* **2002**, *297*, 1160.

(24) Nie, L.; Chen, M.; Sun, X.; Rong, P.; Zheng, N.; Chen, X. *Nanoscale* **2013**.

(25) Baffou, G.; Quidant, R. *Laser Photon. Rev.* **2013**, *7*, 171.

(26) Cook, J. R.; Frey, W.; Emelianov, S. *Acs Nano* **2013**, *7*, 1272.

(27) Orendorff, C. J.; Murphy, C. J. *J. Phys. Chem. B* **2006**, *110*, 3990.

(28) Liu, T.; Thierry, B. *Langmuir* **2012**, *28*, 15634.

(29) Liu, T.; Cousins, A.; Chien, C. C.; Kempson, I.; Thompson, S.; Hwu, Y.; Thierry, B. *Cancer Letters* **2013**, *328*, 271.

(30) Dreaden, E. C.; Alkilany, A. M.; Huang, X. H.; Murphy, C. J.; El-Sayed, M. A. *Chemical Society Reviews* **2012**, *41*, 2740.

(31) Huang, X.; El-Sayed, I. H.; El-Sayed, M. A. *Methods in molecular biology (Clifton, N.J.)* **2010**, *624*, 343.

(32) Ng, V. W. K.; Berti, R.; Lesage, F.; Kakkar, A. *J. Mat. Chem. B* **2013**, *1*, 9.

(33) Fehm, T.; Becker, S.; Duerr-Stoerzer, S.; Sotlar, K.; Mueller, V.; Wallwiener, D.; Lane, N.; Solomayer, E.; Uhr, J. *Breast Cancer Res* **2007**, *9*, R74.

(34) Meng, S. D.; Tripathy, D.; Shete, S.; Ashfaq, R.; Haley, B.; Perkins, S.; Beitsch, P.; Khan, A.; Euhus, D.; Osborne, C.; Frenkel, E.; Hoover, S.; Leitch, M.; Clifford, E.; Vitetta, E.; Morrison, L.; Herlyn, D.; Terstappen, L.; Fleming, T.; Fehm, T.; Tucker, T.; Lane, N.; Wang, J. Q.; Uhr, J. *Proceedings of the National Academy of Sciences of the United States of America* **2004**, *101*, 9393.

(35) Capala, J.; Bouchelouche, K. *Current opinion in oncology* **2010**, *22*, 559.

(36) Hainfeld, J. F.; O'Connor, M. J.; Dilmanian, F. A.; Slatkin, D. N.; Adams, D. J.; Smilowitz, H. M. *Br J Radiol* **2011**, *84*, 526.

(37) Li, P. C.; Wang, C. R.; Shieh, D. B.; Wei, C. W.; Liao, C. K.; Poe, C.; Jhan, S.; Ding, A. A.; Wu, Y. N. *Opt Express* **2008**, *16*, 18605.

(38) Thierry, B.; Al-Ejeh, F.; Brown, M. P.; Majewski, P.; Griesser, H. J. *Adv. Mater.* **2009**, *21*, 541.

(39) Thierry, B.; Griesser, H. J. *Journal of Materials Chemistry* **2012**, *22*, 8810.